UC San Diego
UC San Diego Previously Published Works

Title
Archaeointensity results spanning the past 6 kiloyears from eastern China and implications for extreme behaviors of the geomagnetic field

Permalink
https://escholarship.org/uc/item/9788r0z0

Journal
Proceedings of the National Academy of Sciences of the United States of America, 114(1)

ISSN
0027-8424

Authors
Cai, Shuhui
Jin, Guiyun
Tauxe, Lisa
et al.

Publication Date
2017-01-03

DOI
10.1073/pnas.1616976114

Peer reviewed

Archaeointensity results spanning the past 6 kiloyears from eastern China: Implications for extreme behaviors of the geomagnetic field

Shuhui Cai[a,b], Guiyun Jin[c], Lisa Tauxe[b,1], Chenglong Deng[a,d], Huafeng Qin[d], Yongxin Pan[d,e], and Rixiang Zhu[a]

[a]State Key Laboratory of Lithospheric Evolution, Institute of Geology and Geophysics, Chinese Academy of Sciences, Beijing 100029, China; [b]Scripps Institution of Oceanography, University of California, San Diego, La Jolla, CA 92093-0220; [c]School of History and Culture, Shandong University, Jinan 250100, China; [d]University of Chinese Academy of Sciences, Beijing 100049, China; and [e]Key Laboratory of the Earth and Planetary Physics, Institute of Geology and Geophysics, Chinese Academy of Sciences, Beijing 100029, China

Contributed by Lisa Tauxe, November 16, 2016 (sent for review July 20, 2016; reviewed by Lennart Vincent de Groot and Monika Korte)

Variations of the Earth's geomagnetic field during the Holocene are important for understanding centennial to millennial-scale processes of the Earth's deep interior and have enormous potential implications for chronological correlations (e.g., comparisons between different sedimentary recording sequences, archaeomagnetic dating). Here, we present 21 robust archaeointensity data points from eastern China spanning the past ~6 kyr. These results add significantly to the published data both regionally and globally. Taking together, we establish an archaeointensity reference curve for Eastern Asia, which can be used for archaeomagnetic dating in this region. Virtual axial dipole moments (VADMs) of the data range from a Holocene-wide low of ~27 to "spike" values of ~166 ZAm² (Z: 10^{21}). The results, in conjunction with our recently published data, confirm the existence of a decrease in paleointensity (DIP) in China around ~2200 BCE. These low intensities are the lowest ever found for the Holocene and have not been reported outside of China. We also report a spike intensity of 165.8 ± 6.0 ZAm² at ~1300 BCE (±300 y), which is either a prelude to or the same event (within age uncertainties) as spikes first reported in the Levant.

archaeomagnetism | geomagnetic spikes | geomagnetic secular variation

Archaeomagnetism is an effective way to understand the variation of the geomagnetic field over periods of centuries to millennia during the Holocene. Large fluctuations of the geomagnetic field over the past few thousands of years have been reported, for example, as archaeomagnetic jerks in Europe (1, 2) and eastern Asia (3, 4), as spikes in the Levant (5–7), Turkey (8), and North America (9), as large decreases in paleointensity (DIPs) [DIPs of Kent and Schneider (10)] at ~3000 BCE and ~2200 BCE as well as a possible local high around 1300 BCE in China both reported by Cai et al. (11, 12). Apparent progress has been made on understanding variations of the geomagnetic field during the Holocene in the past few years (13). However, detailed pictures of the global field remain indistinct. Therefore, large numbers of globally distributed data of the highest quality are necessary to further characterize the features of the geomagnetic field. However, the existing paleointensity data from eastern Asia, especially those considered to be "high quality" (passing strict criteria), are sparse. In this study, we carried out detailed rock magnetic and paleointensity studies on samples collected from eastern China spanning the last 6 kyr; these will supplement the published dataset of this area significantly and provide further context for the elusive features of the geomagnetic field mentioned above.

Materials and Methods

The artifacts studied in this paper come from four locations in eastern China, including Shandong, Liaoning, Zhejiang, and Hebei provinces (Fig. 1A). We investigated various materials varying from pottery and porcelain sherds to bricks (Fig. 1 B–E) collected from living sites and kilns, whose ages span the past ~6 kyr. The detailed sampling background and the list of sample

information are in Supporting Information, Archaeomagnetic Background and Sampling, and Table S1. Rock magnetic experiments, including hysteresis loops, isothermal remanent magnetization (IRM) acquisition curves, first-order reversal curves (FORCs), variation of magnetization versus temperature (M–T), and scanning electron microscope (SEM) images as well as elemental spectrum analysis, were conducted on representative samples. The "IZZI" paleointensity protocol (14), as well as partial thermal remanent magnetization (pTRM) checks (15), total TRM anisotropy correction (16), and cooling rate correction (17), was adopted in this study. The detailed experimental procedures can be found in Supporting Information, Experimental Procedures.

Results

The rock magnetic results (Figs. S1–S3; Supporting Information, Rock Magnetic Results) indicate thermally stable fine-grained magnetite and titanium (Ti)- and/or aluminum (Al)-substituted magnetite as the dominant magnetic carriers for most samples, which suggest the suitability of these samples for paleointensity experiments. To obtain the most robust paleointensity data, we need to select the results based on a series of criteria [Paterson

> ### Significance
>
> The geomagnetic field is an intriguing fundamental physical property of the Earth. Its evolution has significant implications for issues such as geodynamics, evolution of the life on the Earth, and archaeomagnetic dating. Here, we present 21 archaeointensity data points from China and establish the first archaeointensity reference curve for eastern Asia. Our results record rarely captured extreme behaviors of the geomagnetic field, with an exceptionally low intensity around ~2200 BCE (hitherto the lowest value observed for the Holocene) and a "spike" intensity value dated at ~1300 ± 300 BCE (either a precursor to or the same event as the Levantine spikes). These anomalous features of the geomagnetic field revealed by our data will shed light on understanding geomagnetic field during the Holocene.

EARTH, ATMOSPHERIC, AND PLANETARY SCIENCES

125
126
127
128
129
130
131
132
133
134
135
136
137
138
139
140
141
142
143
144
145
146
147
148
149
150
151
152
153
154
155
156
157
158
159
160
161
162
163
164
165
166
167
168
169
170
171
172
173
174
175
176
177
178
179
180
181
182
183
184
185
186

187
188
189
190
191
192
193
194
195
196
197
198
199
200
201
202
203
204
205
206
207
208
209
210
211
212
213
214
215
216
217
218
219
220
221
222
223
224
225
226
227
228
229
230
231
232
233
234
235
236
237
238
239
240
241
242
243
244
245
246
247
248
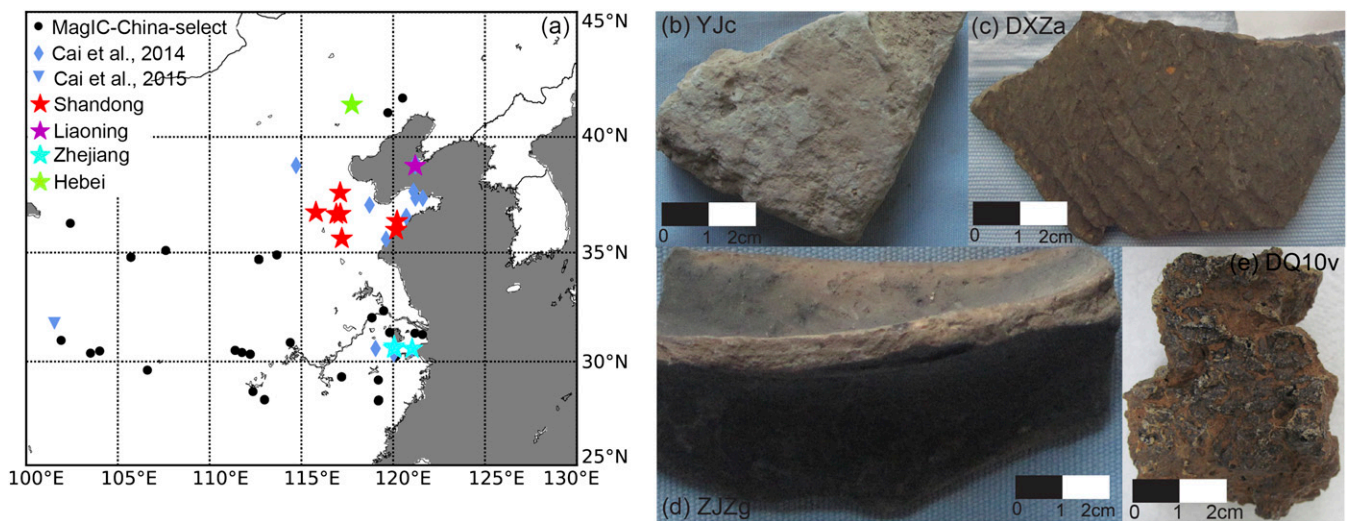
Fig. 1. (A) Site map of this study and the published data from China. Red/magenta/cyan/green stars are the locations of Shandong/Liaoning/Zhejiang/Hebei in this study. Light blue diamonds and downward-pointing triangles represent data locations published by Cai et al. (11, 12). Black solid circles represent locations of the archaeointensity data in China from the MagIC database after data selection. For data selection criteria, please see the text. (B–E) Various archaeomagnetic artifacts analyzed in this study, including brick from Yinjia site, Dezhou, Shandong (B); pottery fragments from Daxinzhuang and Zhaojiazhuang sites in Shandong (C and D); and slag from Laoshushan site, Huzhou, Zhejiang (E).

et al. (18)], for example, those suggested by Shaar and Tauxe (19). The selection statistics used in this study are listed in Table S2. Based on these, 97 specimens from 21 samples out of 407

specimens from 72 samples are considered to yield robust paleointensity estimates. The accepted results at the sample level are listed in Table S3, whereas those at the specimen level are
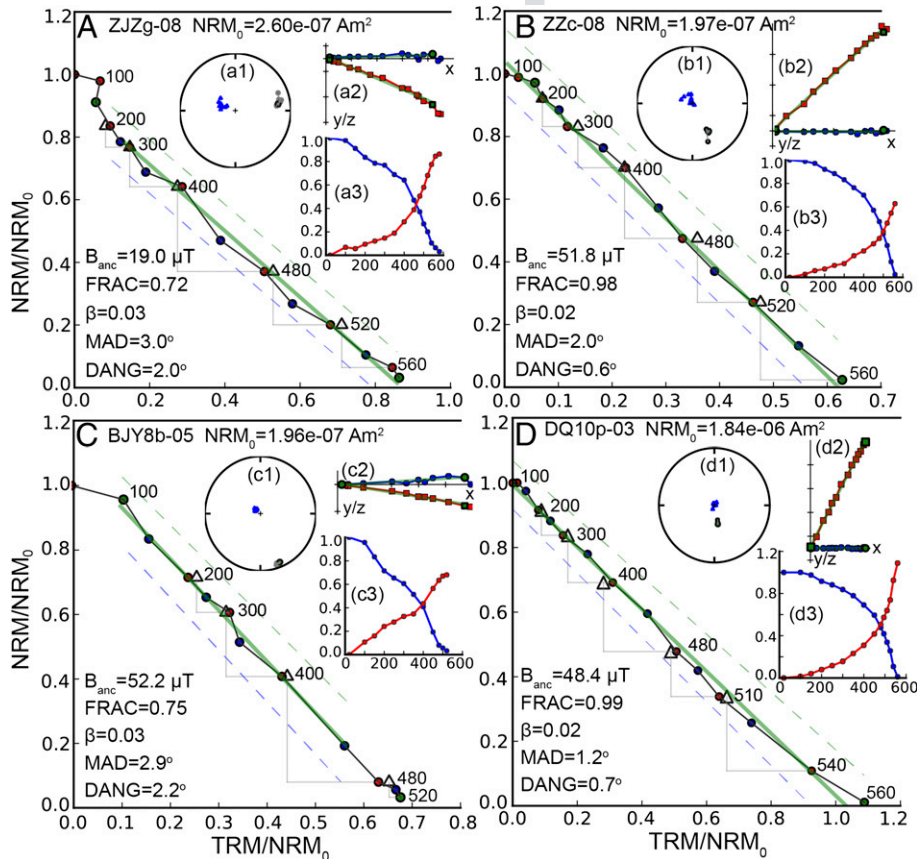
Fig. 2. Arai plots and the associated equal area projections (A1–D1), orthogonal projections (A2–D2), and natural remanent magnetization (NRM) lost-TRM gained curves (A3–D3) of representative accepted specimens. Numbers on the Arai plot and orthogonal projections are temperature steps in centigrade (degrees Celsius). The plots are made with the software of Thellier_GUI (19). For detailed description of these plots, please see the reference.

Q:44
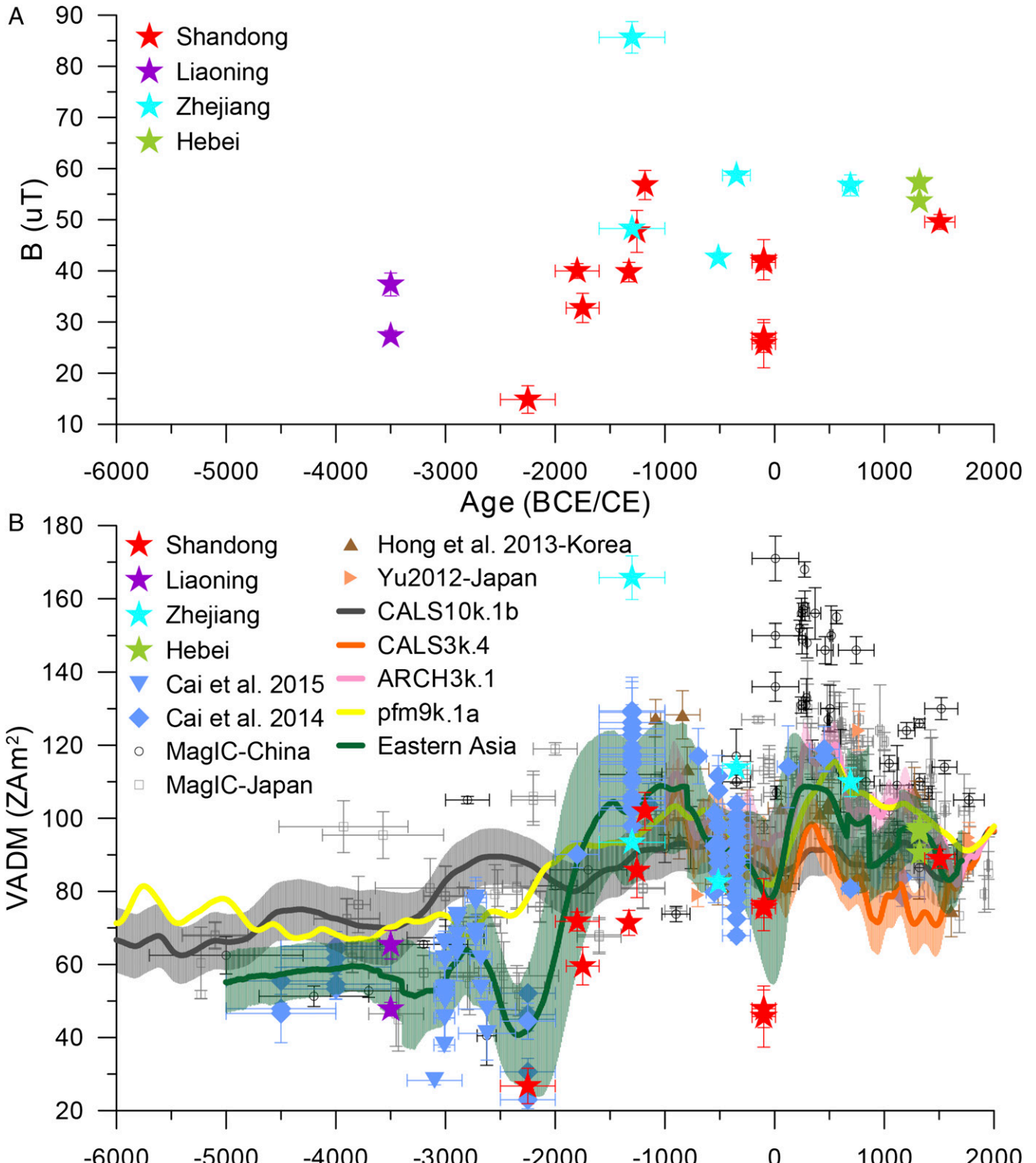
Fig. 3. (*A*) Paleointensity results at the sample level obtained in this study. The red/magenta/cyan/green stars represent data points from Shandong/Liaoning/ Zhejiang/Hebei. (*B*) Comparison of the VADMs in this study with the published data in eastern Asia and predictions from the global models. Light blue di- amonds and downward-pointing triangles are published data in Cai et al. (11, 12). Black circles/squares are the selected published data in China/Japan from the MagIC database. Peach rightward-pointing triangles and brown triangles are recently published data from Japan/Korea (4, 20). The gray/orange/pink/ yellow lines are the predictions from global models of CALS10k.1b (25)/CALS3k.4 (24)/ARCH3k.1 (22)/pfm9k.1a (23), respectively, evaluated at the center of China (35°N, 105°E). The green line is the running average curve of Eastern Asia (calculated with our data and recently published data (4, 11, 12, 20)], whereas the shading represents 1 SD in the bootstrapped results.

Q:45

Q:46

listed in Table S4. Fig. 2 *A*–*D* shows representative plots of accepted specimens; these generally show good linearity on the Arai plots and have a single directional component going straight to the origin except for a limited secondary component removed by 100–150 °C in the orthogonal projection plots (Fig. 2 *A2*–*D2*). The anisotropy and cooling rate corrections are shown in Fig. S4. Alterations of the samples during the anisotropy correction experiments are all less than 8% except one over 10% (Fig. S4*A*), whereas those during cooling rate correction are all limited, with the percentage values of less than 3% (Fig. S4*C*). The ratios of maximum and minimum eigenvalues of the ATRM tensors (τ_1/τ_3) vary between 1.02 and ~2.25 (~82% of them are less than 1.5). The extent of anisotropy correction is generally between 0.9 and 1.1 (Fig. S4*B*) with some exceptions of ~0.65 and 1.3, whereas the cooling rate correction is generally less than 8% (Fig. S4*D*).

The paleointensity values determined for four locations range from 14.8 to 85.7 µT (Fig. 3*A*). The data transformed to virtual axial dipole moments (VADMs) (Fig. 3*B*) range from ~27 to ~166 ZAm^2.

Discussion and Conclusions

Compilation of the Regional Model of Eastern Asia. Here, we present 21 archaeointensity data points from eastern China spanning the past ~6 kyr. We compare our results with those published from eastern Asia that met minimal acceptance criteria (only those obtained through a double-heating protocol, based on averages of at least three specimens and with an SD of mean intensity less than 10% or 5 µT), allowing us to detect the regional variation of the geomagnetic field (Fig. 3*B*). Our data are generally in good agreement with published data from eastern Asia at similar time periods, especially with those data published recently (4, 11, 12, 20). However, we document larger field variations including extremely low (~27 ZAm^2) and high (~166 ZAm^2) values. Combining our data with those recently published (4, 11, 12, 20), we calculated the paleointensity variation curves (green line in Fig. 3*B*) using a parametric bootstrap technique similar to that used by Gallet et al. (21). We resampled 1,000 times at each data point considering uncertainties of both age and VADM, and then applied a running average with a time window of 200 y shifted by 10 y on the dataset (only time intervals including more than three data points were calculated). The established curve is a composite archaeointensity reference curve for eastern Asia, which has applications for archaeomagnetic dating in this area. The data for this curve can be found in Table S5.

Our revised eastern Asian curve agrees well with the ARCH3k.1 (22) and pfm9k.1a (23) models over the past 3 kyr, but deviates from the older CALS3k.4 (24) and CALS10k.1b (25) models at certain time periods, perhaps because of the effect of including sedimentary data in the CALS type models, which are not absolute and are difficult to calibrate (26) and may be overly smoothed. At ages older than ~3 ka, both CALS10k.1b and pfm9k.1a models are in poor agreement with our data, especially when the field reaches the minima at ~3000 BCE and ~2200 BCE and the local maxima around 1300 BCE (Fig. 3*B*). Our data therefore have the potential for greatly improving future global field models.
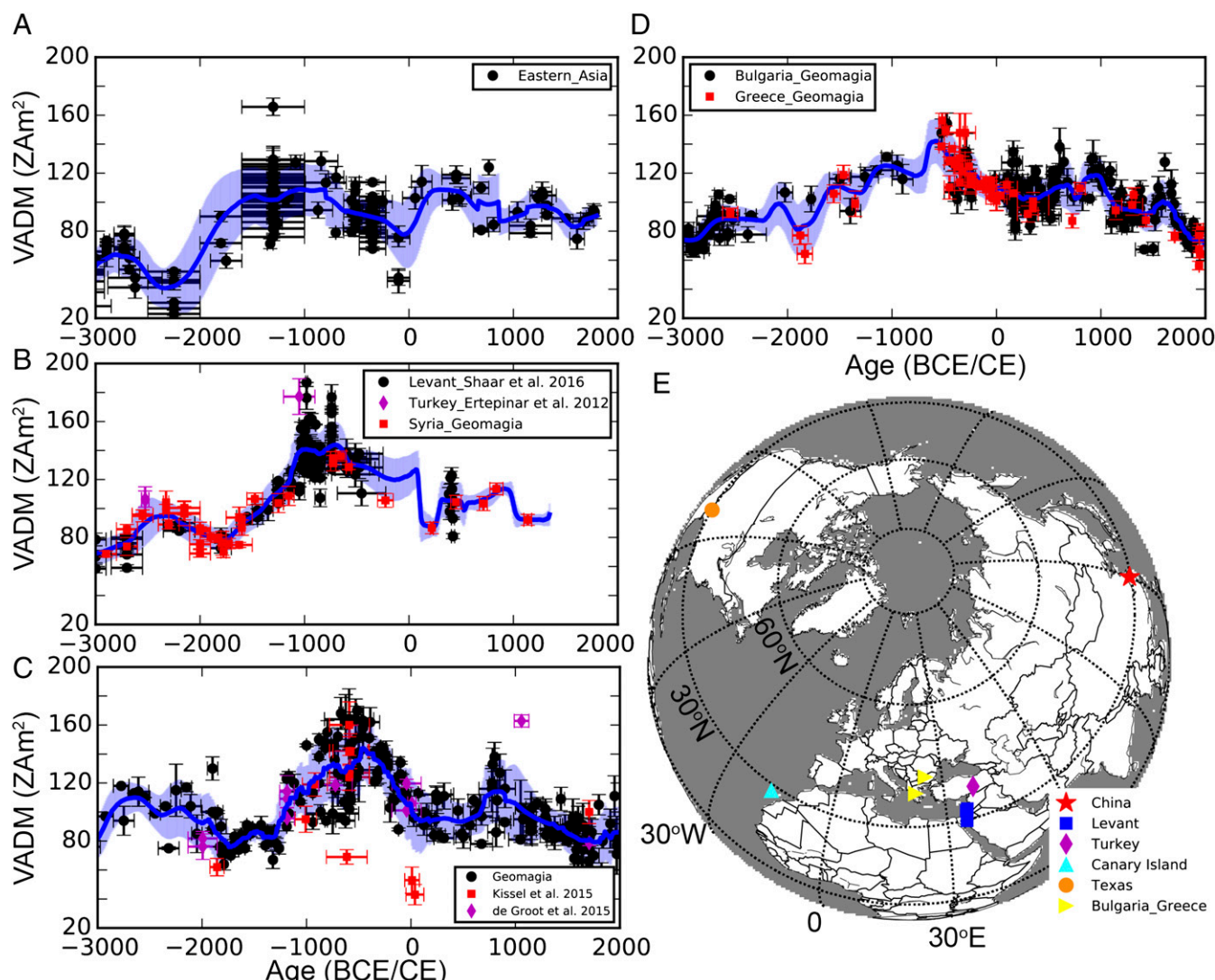
Extreme Behaviors of the Geomagnetic Field. Cai et al. (11) reported two extreme low intensities with VADMs equal to or less than 30 ZAm^2 at ~2200 BCE from Liangchengzhen (LCZ) and Zhaojiangzhuang (ZJZ) site in Shandong. Our results record another low-intensity value (~26.7 ZAm^2) from the ZJZ site. Including the data from Sichuan reported by Cai et al. (12), we now have recorded four low-intensity values from three different sampling sites in total. Taken together, these data strongly support the existence of periods of very low paleointensity or "DIPs" in China at ~3000 BCE and ~2200 BCE, especially at the latter period. These low intensities are the lowest yet determined from
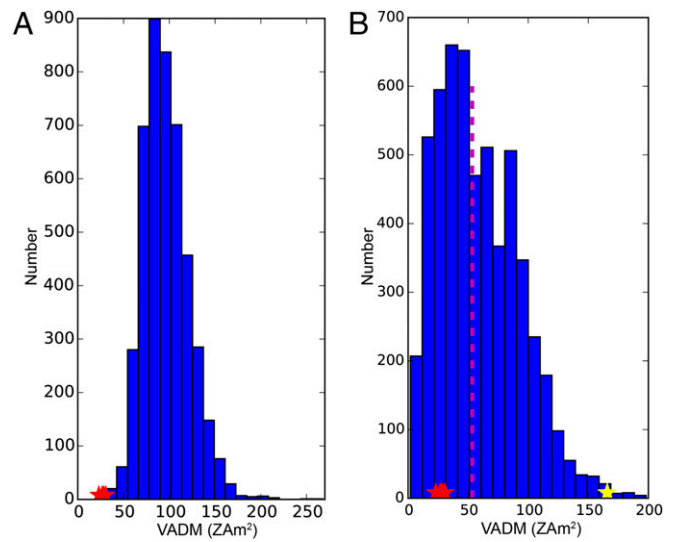
Fig. 4. Histograms of published paleointensity data (blue bars) during the past 10 kyr from GEOMAGIA50.v3 database (39) (*A*) and during the past 200 Ma (not including data from the recent 10 kyr) from the MagIC database (*B*). Red and yellow stars are the extremely low and high values reported from China. The dashed magenta line in *B* represents median value of the data during the past 200 Ma.

any study anywhere for the Holocene (Fig. 4*A*), which can be either a local geomagnetic anomaly or not captured in other areas. This calls for additional widely distributed data at similar time periods to further characterize their global features and geodynamic mechanisms.

In addition to periods of extremely low field intensities, Cai et al. (11) reported a period of possible high field intensity dated around 1300 BCE (±300 y). Here, we obtained additional samples from the same sites and find an even higher value of ~165.8 ZAm^2 (Figs. 3*B* and 5*A*), which meets the definition of a "spike" suggested by Cai et al. (11) of fields in excess of 160 ZAm^2 and is nearly as high as those reported in the Levant around 980 BCE (5–7) and in Turkey at ~1050 BCE (8) (Fig. 5*B*), but the median age is some 300 y earlier (although there is a large uncertainty in the age of ~300 y). The high value recorded by our data could represent a spike around 1300 BCE in China, which might be a precursor to those recorded in the Levant and Turkey. A high intensity of ~160 ZAm^2 was reported by de Groot et al. (27) in Canary Islands, whose age is 1058 CE based on radiocarbon dating (28) and could alternatively be ~400–300 BCE constrained by the variation curve of the geomagnetic direction. Under the latter scenario, they suggested a westward motion of the Levantine spikes. In addition, Kissel et al. (29) reported high intensities with VADMs over 160 ZAm^2 in Gran Canaria and locations nearby (e.g., Portugal, Spain, and the Azores) between 670 BCE and 400 BCE (Fig. 5*C*). It seems our data support this speculation that the spike first appeared in China at ~1300 BCE and then migrated westward to the Levant at ~1000 BCE and finally to Europe at ~670–400 BCE (Fig. 5*E*). However, the age errors of the Chinese spike overlap with the Levantine spike and could instead represent the same event. Under this interpretation, the spike intensity recorded by our data extends the spatial distribution of the spike reported in Levantine area and Turkey to Eastern Asia. It is interesting to note that Bourne et al. (9) reported a possible spike in sediments at ~3 ka in Texas, implying that the spike could be a global feature or that there are at least two large flux lobes simultaneously (Fig. 5*E*). We note, however, that the spike at ~1000 BCE has so far not been not seen in European [e.g., Bulgaria and Greece (Fig. 5*D*)], or even

497
498
499
500
501
502
503
504
505
506
507
508
509
510
511
512
513
514
515
516
517
518
519
520
521
522
523
524
525
526
527
528
529
530
531
532
533
534

Fig. 5. (A–D) Composite curves from representative areas: A includes only the eastern Asian data published recently (4, 11, 12, 20); B includes all of the Levantine data compiled by Shaar et al. (7), the data in Turkey published by Ertepinar et al. (8), and data in Syria from the Geomagia50.v3 database; C includes data within a 2,000-km-radius circle around Canary Island from the Geomagia50.v3 database compiled by Kissel et al. (29) and data published recently by Kissel et al. (29) and de Groot et al. (27); D includes data in Bulgaria and Greece from the Geomagia50.v3 database. The selection criteria of including at least three specimens and with a SD of mean intensity less than 10% or 5 μT were applied on these data. (E) Projections of the locations related to geomagnetic spikes.

Syrian data (Fig. 5B) at similar period. These imply that the spike is likely not global but probably large scale, which fulfills one of the conditions for generating such a spike in numerical modeling (30). However, the composite curves in Fig. 5 show that the field intensity is overall high around 1000–500 BCE at different areas, indicating a dipolar behavior of the field. Taken together, the different records of the spike suggest that it is probably a nondipolar event superimposed on an already strong dipolar field. This speculation is similar to the deduction by de Groot et al. (31) that strong, short-term intensity perturbations are superimposed on a global trend of dipolar decay over the past 1 kyr. This indicates that the variation of the pattern of the geomagnetic field, at least during the past 3 kyr, is possibly driven by the dipole component on which nondipole components superpose occasionally (13). In any case, further data with large spatial distributions and precise age constraints are necessary for achieving an improved understanding of this extreme behavior of the geomagnetic field.

The DIP and spike confirmed by our results suggest a large [eightfold increase if calculating with the low intensity of

~20 ZAm^2 reported by Cai et al. (11) and our high value of ~166 ZAm^2] and rapid (within ~1,000 y) fluctuations of the geomagnetic field during the Holocene. Our extreme intensity values are still striking, even when placed in a context of the past 200 Ma. The low values of our data (red stars in Fig. 4B) fall into low end of intensities in the published data and are lower than the median intensity (~54 ZAm^2) of the past 200 Ma (not including data from the recent 10 kyr). Our low intensities are comparable to the strength of the field during some particular geomagnetic intervals, for example, the Laschamp geomagnetic excursion (32) and the Miocene dipole low (33, 34). Our spike (yellow star in Fig. 4B) is among the highest paleointensities recorded over the past 200 Ma. In summary, the extreme behaviors recorded by our data are extraordinary, especially when considering the short span of the record, and thus bring challenges to geodynamical modeling (30, 35–38).

1. Gallet Y, Genevey A, Courtillot V (2003) On the possible occurrence of "archaeomagnetic jerks" in the geomagnetic field over the past three millennia. *Earth Planet Sci Lett* 214(1-2):237–242.
2. Snowball I, Sandgren P (2004) Geomagnetic field intensity changes in Sweden between 9000 and 450 cal BP: Extending the record of "archaeomagnetic jerks" by means of lake sediments and the pseudo-Thellier technique. *Earth Planet Sci Lett* 227: 361–376.
3. Yu Y, et al. (2010) Archeomagnetic secular variation from Korea: Implication for the occurrence of global archeomagnetic jerks. *Earth Planet Sci Lett* 294(1-2):173–181.
4. Yu Y (2012) High-fidelity paleointensity determination from historic volcanoes in Japan. *J Geophys Res* 117(B8):8101.
5. Ben-Yosef E, et al. (2009) Geomagnetic intensity spike recorded in high resolution slag deposit in Southern Jordan. *Earth Planet Sci Lett* 287(3-4):529–539.
6. Shaar R, et al. (2011) Geomagnetic field intensity: How high can it get? How fast can it change? Constraints from Iron Age copper slag. *Earth Planet Sci Lett* 301(1-2): 297–306.
7. Shaar R, et al. (2016) Large geomagnetic field anomalies revealed in Bronze to Iron Age archeomagnetic data from Tel Megiddo and Tel Hazor, Israel. *Earth Planet Sci Lett* 442:173–185.
8. Ertepinar P, et al. (2012) Archaeomagnetic study of five mounds from Upper Mesopotamia between 2500 and 700 BCE: Further evidence for an extremely strong geomagnetic field ca. 3000 years ago. *Earth Planet Sci Lett* 357-358:84–98.
9. Bourne MD, et al. (2016) High-intensity geomagnetic field "spike" observed at ca. 3000 cal BP in Texas, USA. *Earth Planet Sci Lett* 442:80–92.
10. Kent DV, Schneider DA (1995) Correlation of paleointensity variation records in the Brunhes/Matuyama polarity transition interval. *Earth Planet Sci Lett* 129(1):135–144.
11. Cai S, et al. (2014) Geomagnetic intensity variations for the past 8 kyr: New archaeointensity results from Eastern China. *Earth Planet Sci Lett* 392:217–229.
12. Cai S, et al. (2015) New constraints on the variation of the geomagnetic field during the late Neolithic period: Archaeointensity results from Sichuan, southwestern China. *J Geophys Res Solid Earth* 120(4):2056–2069.
13. Constable C, Korte M (2015) Centennial- to millennial-scale geomagnetic field variations. *Treatise on Geophysics*, ed Schubert G (Elsevier, Amsterdam), 2nd Ed, Vol 5, pp 309–341.

Q:39

14. Tauxe L, Staudigel H (2004) Strength of the geomagnetic field in the Cretaceous Normal Superchron: New data from submarine basaltic glass of the Troodos Ophiolite. *Geochem Geophys Geosyst* 5(2):Q02H06.
15. Coe RS, Grommé S, Mankinen EA (1978) Geomagnetic paleointensities from radiocarbon-dated lava flows on Hawaii and the question of the Pacific nondipole low. *J Geophys Res Solid Earth* 83(B4):1740–1756.
16. Veitch RJ, Hedley IG, Wagner JJ (1984) An investigation of the intensity of the geomagnetic field during Roman times using magnetically anisotropic bricks and tiles. *Arch Sci Genève* 37(3):359–373.
17. Genevey A, Gallet Y (2002) Intensity of the geomagnetic field in Western Europe over the past 2000 years: New data from French ancient pottery. *J Geophys Res* 107(B11): 2285.

Q:40

18. Paterson GA, Tauxe L, Biggin AJ, Shaar R, Jonestrask LC (2014) On improving the selection of Thellier-type paleointensity data. *Geochem Geophys Geosyst* 15(4): 1180–1192.
19. Shaar R, Tauxe L (2013) Thellier GUI: An integrated tool for analyzing paleointensity data from Thellier-type experiments. *Geochem Geophys Geosyst* 14(3):677–692.
20. Hong H, et al. (2013) Globally strong geomagnetic field intensity circa 3000 years ago. *Earth Planet Sci Lett* 383:142–152.
21. Gallet Y, et al. (2015) New Late Neolithic (c. 7000–5000 BC) archeointensity data from Syria. Reconstructing 9000 years of archeomagnetic field intensity variations in the Middle East. *Phys Earth Planet Inter* 238:89–103.
22. Korte M, Donadini F, Constable CG (2009) Geomagnetic field for 0–3 ka: 2. A new series of time-varying global models. *Geochem Geophys Geosyst* 10(6):Q06008.
23. Nilsson A, Holme R, Korte M, Suttie N, Hill M (2014) Reconstructing Holocene geomagnetic field variation: New methods, models and implications. *Geophys J Int* 198(1):229–248.

24. Korte M, Constable C (2011) Improving geomagnetic field reconstructions for 0-3 ka. *Phys Earth Planet Inter* 188(3-4):247–259.
25. Korte M, Constable C, Donadini F, Holme R (2011) Reconstructing the Holocene geomagnetic field. *Earth Planet Sci Lett* 312(3-4):497–505.
26. Tauxe L, Steindorf JL, Harris A (2006) Depositional remanent magnetization: Toward an improved theoretical and experimental foundation. *Earth Planet Sci Lett* 244(3-4): 515–529.
27. de Groot LV, et al. (2015) High paleointensities for the Canary Islands constrain the Levant geomagnetic high. *Earth Planet Sci Lett* 419:154–167.
28. Carracedo JC, et al. (2007) Eruptive and structural history of Teide Volcano and rift zones of Tenerife, Canary Islands. *Geol Soc Am Bull* 119(9-10):1027–1051.
29. Kissel C, et al. (2015) Holocene geomagnetic field intensity variations: Contribution from the low latitude Canary Islands site. *Earth Planet Sci Lett* 430:178–190.
30. Livermore PW, Fournier A, Gallet Y (2014) Core-flow constraints on extreme archeomagnetic intensity changes. *Earth Planet Sci Lett* 387:145–156.
31. de Groot LV, Biggin AJ, Dekkers MJ, Langereis CG, Herrero-Bervera E (2013) Rapid regional perturbations to the recent global geomagnetic decay revealed by a new Hawaiian record. *Nat Commun* 4:2727.
32. Laj C, Guillou H, Kissel C (2014) Dynamics of the earth magnetic field in the 10–75 kyr period comprising the Laschamp and Mono Lake excursions: New results from the French Chaîne des Puys in a global perspective. *Earth Planet Sci Lett* 387:184–197.
33. Tauxe L, Gee JS, Steiner MB, Staudigel H (2013) Paleointensity results from the Jurassic: New constraints from submarine basaltic glasses of ODP Site 801C. *Geochem Geophys Geosyst* 14(10):4718–4733.
34. Sprain CJ, Feinberg JM, Geissman JW, Strauss B, Brown MC (2015) Paleointensity during periods of rapid reversal: A case study from the Middle Jurassic Shamrock batholith, western Nevada. *Geol Soc Am Bull* 128:223–238.
35. Brown MC, Korte M (2016) A simple model for geomagnetic field excursions and inferences for palaeomagnetic observations. *Phys Earth Planet Inter* 254:1–11.
36. Tarduno JA, et al. (2015) Antiquity of the South Atlantic Anomaly and evidence for top-down control on the geodynamo. *Nat Commun* 6:7865.

Q:41

37. Finlay CC, Aubert J, Gillet N (2016) Gyre-driven decay of the Earth's magnetic dipole. *Nat Commun* 7:10422.
38. Aubert J, Finlay CC, Fournier A (2013) Bottom-up control of geomagnetic secular variation by the Earth's inner core. *Nature* 502(7470):219–223.
39. Brown MC, et al. (2015) GEOMAGIA50.v3: 1. General structure and modifications to the archeological and volcanic database. *Earth Planets Space* 67:83.

Q:42

40. Luan FS, Wagner M (2009) The chronology and basic developmental sequence of archaeological cultures in the Haidai Region. *Chinese Archaeology and Palaeoenvironment I*, eds Wagner M, Luan FS, Tarasov P (Philipp von Zabern, Mainz, Germany), pp 1–16.
41. Liu X, et al. (2016) The virtues of small grain size: Potential pathways to a distinguishing feature of Asian wheats. *Quatern Int*, in press.

Q:43

42. Tauxe L, Mullender TAT, Pick T (1996) Potbellies, wasp-waists, and superparamagnetism in magnetic hysteresis. *J Geophys Res* 101(B1):571–583.
43. Tauxe L, Banerjee SK, Butler RF, van der Voo R (2010) *Essentials of Paleomagnetism* (Univ of California Press, Berkeley), pp 143–146.
44. Roberts AP, Pike CR, Verosub KL (2000) First-order reversal curve diagrams: A new tool for characterizing the magnetic properties of natural samples. *J Geophys Res Solid Earth* 105(B12):28461–28475.
45. Pike CR, Roberts AP, Verosub KL (2001) First-order reversal curve diagrams and thermal relaxation effects in magnetic particles. *Geophys J Int* 145:721–730.
46. Chauvin A, Garcia Y, Lanos P, Laubenheimer F (2000) Paleointensity of the geomagnetic field recovered on archaeomagnetic sites from France. *Phys Earth Planet Inter* 120(1-2):111–136.
47. Mitra R, Tauxe L, Keech McIntosh S (2013) Two thousand years of archeointensity from West Africa. *Earth Planet Sci Lett* 364:123–133.
48. Jiang Z, et al. (2014) Thermal magnetic behaviour of Al-substituted haematite mixed with clay minerals and its geological significance. *Geophys J Int* 200(1):130–143.
49. Harrison RJ, Feinberg JM (2008) FORCinel: An improved algorithm for calculating first-order reversal curve distributions using locally weighted regression smoothing. *Geochem Geophys Geosyst* 9(5):Q05016.

AUTHOR QUERIES

AUTHOR PLEASE ANSWER ALL QUERIES 1

Q: 1_Please contact PNAS_Specialist.djs@sheridan.com if you have questions about the editorial changes, this list of queries, or the figures in your article. Please include your manuscript number in the subject line of all email correspondence; your manuscript number is 201616976.

Q: 2_Please (i) review the author affiliation and footnote symbols carefully, (ii) check the order of the author names, and (iii) check the spelling of all author names, initials, and affiliations. Please check with your coauthors about how they want their names and affiliations to appear. To confirm that the author and affiliation lines are correct, add the comment "OK" next to the author line. This is your final opportunity to correct any errors prior to publication. Misspelled names or missing initials will affect an author's searchability. Once a manuscript publishes online, any corrections (if approved) will require publishing an erratum; there is a processing fee for approved erratum.

Q: 3_Please review and confirm your approval of the short title: Chinese archaeomagnetism: The last 6 kyr. If you wish to make further changes, please adhere to the 50-character limit. (NOTE: The short title is used only for the mobile app and the RSS feed.)

Q: 4_Please review the information in the author contribution footnote carefully. Please make sure that the information is correct and that the correct author initials are listed. Note that the order of author initials matches the order of the author line per journal style. You may add contributions to the list in the footnote; however, funding should not be an author's only contribution to the work.

Q: 5_You have chosen not to pay an additional $1350 (or $1000 if your institution has a site license) for the PNAS open access option. Please confirm this is correct and note your approval in the margin.

Q: 6_Please verify that all callouts for supporting information (SI) in text are correct. Note, however, that the hyperlinks for SI callouts will not work until the article is published online. In addition, SI that is not composed in the main SI PDF (appendices, datasets, movies, and "Other Supporting Information Files") have not been changed from your originally submitted file and so are not included in this set of proofs. The proofs for any composed portion of your SI are included in this proof as subsequent pages following the last page of the main text. If you did not receive the proofs for your SI, please contact **PNAS_Specialist.djs@sheridan.com**.

Q: 7_PNAS allows up to five keywords. You may add two keywords. Also, please check the order of your keywords and approve or reorder them as necessary.

Q: 8_Per PNAS style, certain compound terms are hyphenated when used as adjectives and unhyphenated when used as nouns. This style has been applied consistently throughout where (and if) applicable.

Q: 9_For article title: PNAS does not allow claims of priority or primacy, hence the term "New" has been deleted from the title.

Q: 10_Please confirm whether all units/divisions/departments/laboratories/sections have been included in the affiliations line for each footnote symbol or add if missing. PNAS requires smallest institutional unit(s) to be listed for each author in each affiliation. Please confirm or correct affiliation addresses.

Q: 11_In sentence beginning "Here, we present 21 archaeointensity data...." (in Significance statement): (i) PNAS does not allow claims of priority or primacy, hence the term "new" has been deleted. (ii) Okay to change "data" to "data points" in this sentence? Please confirm or correct.

Q: 12_In sentence beginning "These results add significantly....": PNAS does not allow claims of priority or primacy, hence the term "new" has been deleted.

Q: 13_In sentence beginning "Taking together, we establish....": PNAS does not allow claims of priority or primacy, hence the term "first" has been deleted.

Q: 14_In sentence beginning "Virtual axial dipole moments....": PNAS does not allow claims of priority or primacy, hence the term "new" has been deleted.

Q: 15_In sentence beginning "The results, in conjunction....": PNAS does not allow claims of priority or primacy, hence the term "new" has been deleted.

Q: 16_Some of the author contribution statements require some clarification and rewriting. In the following, could you please (i) identify who is meant by "L.T. the first author"; (ii) identify who is meant by "the first author" elsewhere; (iii) identify who is meant by "my" and "I"; and (iv) spell out "postdoc": "G.J. provided archaeological samples and age constraints; L.T. the first author is a postdoc in my laboratory; I have participated in all of the analyses conducted there and helped with data analysis and writing of the manuscript; C.D. provided mentorship and support of the first author; H.Q. provided assistance in the Beijing paleomagnetic laboratory for analyses; Y.P. provided mentorship of the first author during the project and helped with manuscript writing; R.Z. provided access to the Beijing laboratory, was primary mentor of the first author during doctoral research, and provided monetary support for the project."

Q: 17_Please note that the Conflict of Interest Statement "One reviewer was minor coauthor of a paper coauthored by L.T. We have a total of three, so two are independent" has been removed per PNAS style.

Q: 18_In Reviewers line: "Potsdam" has been changed to "University of Potsdam." Please confirm change.

Q: 19_For Data deposition footnote: (i) The data deposition statement was also included in *Acknowledgments*, but a different URL was listed in *Acknowledgments*: "https://earthref.org/MagIC/11131/." The redundant statement has been removed from *Acknowledgments*. Could you please verify whether the URL should be changed in the Data deposition footnote? (ii) Okay to spell out "paleo-" as "paleomagnetic" in the following sentence: "This is the primary database for

AUTHOR QUERIES

all paleomagnetic and rock magnetic data"? Please confirm. (iii) Please indicate whether the sequences have been deposited in MagIC or another publicly accessible database before your page proofs are returned. It is PNAS policy that the data be deposited BEFORE the paper can be published.

Q: 20 Please note that, per journal style, all of the citations of "*SI Appendix*" have been changed to "*Supporting Information*" in this article.

Q: 21 In the sentence beginning "Here, we present....": PNAS does not allow claims of priority or primacy, hence the term "new" has been deleted.

Q: 22 In sentence beginning "We compare our results....": PNAS does not allow claims of priority or primacy, hence the term "new" has been deleted.

Q: 23 In sentence beginning "Our data are generally....": PNAS does not allow claims of priority or primacy, hence the term "new" has been deleted.

Q: 24 In sentence beginning "Combining our data....": PNAS does not allow claims of priority or primacy, hence the term "new" has been deleted.

Q: 25 In sentence beginning "We resampled 1,000 times....": PNAS does not allow claims of priority or primacy, hence the term "new" has been deleted.

Q: 26 In sentence beginning "To our knowledge, the established curve is the first....": PNAS does not allow claims of priority or primacy, hence the term "first" has been deleted.

Q: 27 In sentence beginning "Our data therefore....": PNAS does not allow claims of priority or primacy, hence the term "new" has been deleted.

Q: 28 In sentence beginning "Our results record another low....": PNAS does not allow claims of priority or primacy, hence the term "new" has been deleted.

Q: 29 Per PNAS style, quotation marks have been used at the first appearance of a word or phrase but have been deleted at each subsequent use of that word or phrase.

Q: 30 In sentence beginning "The high value recorded....": PNAS does not allow claims of priority or primacy, hence the term "new" has been deleted.

Q: 31 In sentence beginning "It seems our data support....": PNAS does not allow claims of priority or primacy, hence the term "new" has been deleted.

Q: 32 In sentence beginning "Under this interpretation....": PNAS does not allow claims of priority or primacy, hence the term "new" has been deleted.

Q: 33 In sentence beginning "The DIP and spike confirmed....": PNAS does not allow claims of priority or primacy, hence the term "new" has been deleted (two times in this sentence).

AUTHOR QUERIES

AUTHOR PLEASE ANSWER ALL QUERIES 4

Q: 34_In sentence beginning "Our extreme intensity values....": PNAS does not allow claims of priority or primacy, hence the term "new" has been deleted.

Q: 35_In sentence beginning "Our spike....": PNAS does not allow claims of priority or primacy, hence the term "new" has been deleted.

Q: 36_In sentence beginning "In summary, the extreme behaviors....": PNAS does not allow claims of priority or primacy, hence the term "new" has been deleted.

Q: 37_In the Acknowledgments, please check the names of persons thanked for assistance/contributions, names of granting agencies, grant numbers, and initials of grant recipients for accuracy.

Q: 38_In *Acknowledgments*: "NSFC" has been defined as "National Natural Science Foundation of China," "NSF" has been spelled out as "National Science Foundation," and "CAS" has been spelled out as "Chinese Academy of Sciences." Please confirm the definitions.

Q: 39_For ref. 13 (Constable and Korte): This reference has been updated. Please confirm location of publisher.

Q: 40_For ref. 17 (Genevey and Gallet): This reference has been updated. Please confirm issue number.

Q: 41_For ref. 36 (Tarduno et al.): This reference has been updated. Please confirm page number (or article ID number).

Q: 42_For ref. 39 (Brown et al.): This reference has been updated. Please confirm page number (or article ID number).

Q: 43_For ref. 41 (Liu et al.): If possible, please update this reference by providing the volume, issue, and page numbers of the article.

Q: 44_In Fig. 2 legend: "NRM" has been defined as "natural remanent magnetization." Please confirm the definition.

Q: 45_In "(*A*) Paleointensity results...." (in Fig. 3 legend): PNAS does not allow claims of priority or primacy, hence the term "new" has been deleted.

Q: 46_In sentence beginning "The green line is...." (in Fig. 3 legend): PNAS does not allow claims of priority or primacy, hence the term "new" has been deleted.

Supporting Information

Archaeomagnetic Background and Sampling

The samples from Shandong province were collected from 10 different sites covering the prehistoric cultures of early Dawenkou (4300–3500 BCE), Longshan (2500–2000 BCE), and Yueshi (2000–1600 BCE), as well as the historical dynasties of middle-late Shang (1300–1000 BCE), Western Han (206 BCE–8 CE), and Ming (1368–1644 CE). To confirm the unusually low paleointensities discovered by Cai et al. (11), we collected pottery shards from the Liangchengzhen (LCZ) and Zhaojiazhuang (ZJZ) sites. The remaining artifacts from Shandong were collected from eight sites. The samples from Liaoning province are all from Wenjiacun (WJC) site located in the Lvshun area, Dalian City, which is dated to the middle Dawenkou (~3500 BCE). All of the samples from Shandong and Liaoning were provided by the archaeologists from the School of History and Culture, Shandong University, Jinan, China. The ages of our sites from prehistoric periods and the DXZ site (middle-late Shang) are based on radiocarbon dating (40, 41) as well as archaeological contexts. The ages of other sites were determined mainly based on archaeological background.

The samples from Zhejiang province were collected from part of the published sites in Cai et al. (11), which cover the dynasties of early Tang (618–764 CE), Zhanguo (475–221 BCE), Late Chunqiu (550–476 BCE), and Shang (1600–1000 BCE). Ages of samples from this site are based on typology of the potteries during archaeological survey.

One site from Hebei province is included, which is the Baojiaying (BJY) site located at Longhua county, Chengde City. This site used to be a big kiln factory started during the Liao-Jin dynasty (907–1125 CE) and terminated in Yuan dynasty (1271–1368 CE). A total of 10 cultural layers were excavated on this site. The materials we collected were from the fourth–fifth layer, where some ancient coins from the Yuan dynasty were unearthed. Combing with the typology of the potteries, our samples collected from this site are dated to the Yuan dynasty.

Besides radiocarbon dating (40, 41) and archaeological dating based on archaeological context (e.g., the workmanship and decoration of the potteries, important information preserved on the artifacts such as the ancient Chinese characters, representative artifacts such as ancient corns correspond to special dynasties), we attempted to use the optically stimulated luminescence (OSL) dating method on nine pottery samples (three from Shandong and six from Zhejiang), but none of them gave acceptable results unfortunately. The detailed sampling information is listed in Table S1.

Experimental Procedures

Rock Magnetism. To determine the magnetic mineralogy of the studied samples, we carried out detailed rock magnetic experiments including hysteresis loops, isothermal remanent magnetization (IRM) acquisition, first-order reversal curves (FORCs), and variation of magnetization versus temperature (M–T). Powder samples (0.1–0.2 g) were prepared and fixed in non-magnetic capsules for the hysteresis loops, IRM acquisition, and FORCs experiment, which were measured with the MicroMag 3900 VSM in the Paleomagnetism and Geochronology Laboratory (PGL) at Institute of Geology and Geophysics, Chinese Academy of Sciences (IGGCAS). M–T curves were measured with the magnetic-measurements variable-field translation balance fixed with an oven in PGL for the purpose of determining Curie temperatures (T_c values) and detecting possible alteration during heating. Microprobe slices (thickness of 30–50 μm) of selected samples were prepared and observed under scanning

electron microscope (SEM). The slices were coated with a carbon layer to prevent surface charging of the sample during SEM operation. The SEM experiments were performed with FEI Nova nano450 at 15-kV acceleration voltages in IGGCAS. The imaging and energy dispersive X-ray spectroscopy (EDS) analyses were conducted under the backscattered electron (BSE) mode.

Paleointensity. A total of 407 specimens from 72 samples (55, 6, 6, and 5 from Shandong, Liaoning, Zhejing, and Hebei, respectively) were processed for paleointensity experiments with a minimum of five specimens per sample. Among all of the specimens, 376 were processed in the PGL, whereas the other 31 were measured in the paleomagnetism laboratory of the Scripps Institution of Oceanography (SIO), University of California, San Diego. For experimental procedure in the PGL, samples were first broken into irregular chips. Then fresh specimens were selected and fixed in cubic ceramic boxes (1.2 cm × 1.2 cm × 1.2 cm), which have comparable magnetic moments to the background of the magnetometer used for the measurements, with fire-resistant cotton matting. The specimens were heated in a French paleointensity furnace in an argon atmosphere and cooled naturally after heating (~12 h). Heating steps were carried out from 100 to 580 °C with temperature intervals varying from 20 to 100 °C. The residual field of the oven is less than 10 nT for the "zero-field" cooling steps and a laboratory field of 30 μT was applied along –z of the specimens with a precision of 0.1 μT for the "in-field" cooling steps. The remanence was measured with the 2G 760 SQUID magnetometer after each step. The whole procedure of the experiment was conducted in a shielded room with residual field less than 300 nT.

In the SIO laboratory, fresh specimens were fixed in 12-mm-diameter glass tubes with glass microfiber paper and potassium-silicate glue (KASIL). Specimens were heated in the laboratory-built paleointensity oven equipped with a fan for cooling. The cooling times to room temperature are about 30–45 min depending on the peak temperature. The residual field of the ovens is less than 10 nT during zero-field steps. Measurements were made on a 2G cryogenic magnetometer. The same heating steps as those in PGL were followed. A laboratory field is applied along –z axis of the specimens, and field value of 30 or 50 μT was chosen depending on the expected ancient field of samples. All of the experiments were conducted in the paleomagnetic shielded room at SIO.

The "IZZI" protocol was followed for all of the specimens during the paleointensity experiment (14). Checks for alteration [partial thermal remanent magnetization (pTRM) checks] were inserted at every other step (15). The bias caused by the anisotropy of TRM (ATRM) in paleointensity for archaeological materials can reach ~10% or more, whereas that caused by cooling rate effect is around 5% with a few exceptions of 15% (11, 12). Therefore, both ATRM and cooling rate effects should be considered when determining the paleointensity values recorded by archaeological artifacts. In this study, the ATRM correction was conducted on each successful specimen in the intensity experiment. An eight-step (baseline, +x, −x, +y, −y, +z, −z, +x) experiment was conducted following the method of Veitch et al. (16), whereby the last step is an alteration check. A total TRM was used for calculation of the anisotropy tensors. Cooling rate corrections were conducted on those specimens heated in the paleointensity ovens in SIO but not on those processed in the French furnace in PGL because the natural cooling system of the latter mimics the original cooling of the pottery when first fired. The cooling rate correction experiment

follows the procedure suggested by Genevey and Gallet (17), including three steps: fast cooling, slow cooling, and a second fast cooling as an alteration check. The slow cooling step takes ~12 h in the SIO ovens. Detailed experimental steps can be found in Cai et al. (11).
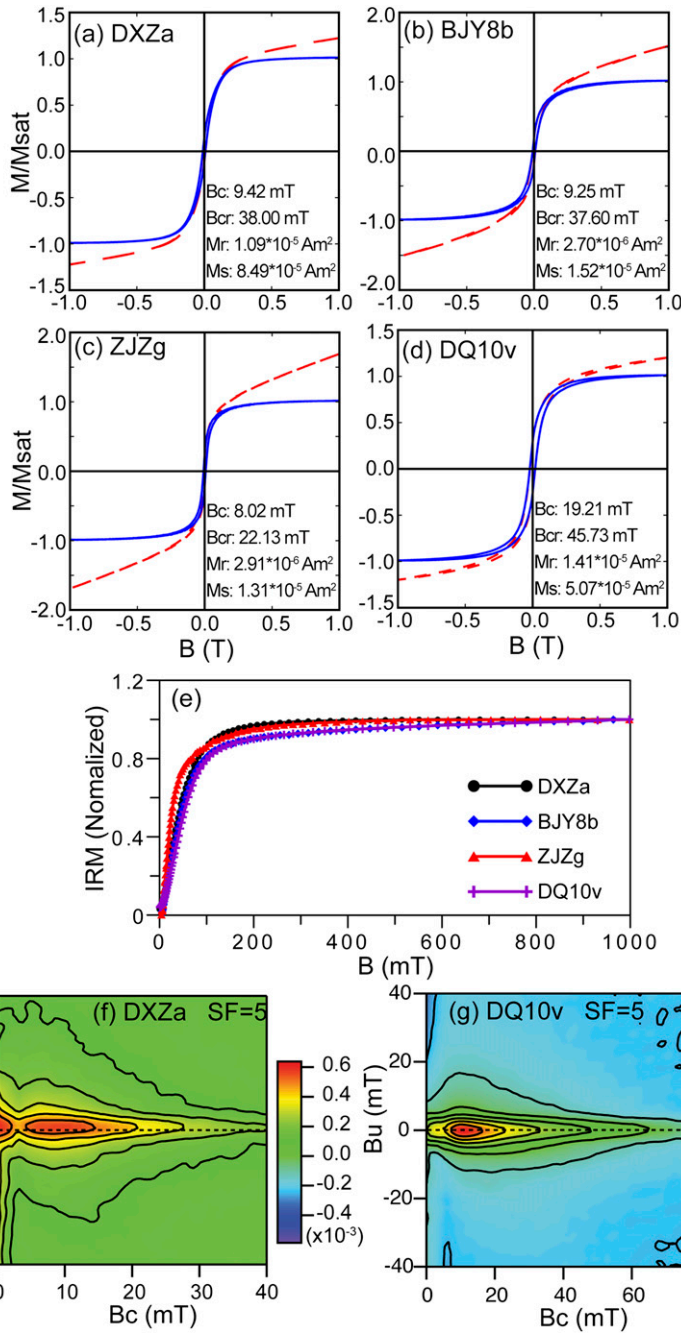
Rock Magnetic Results

The representative hysteresis loops show slightly "wasp-waisted" shapes (Fig. S1 *B* and *C*), suggesting a mixing of either SD and SP grain sizes (42) or varied magnetic minerals (e.g., magnetite and hematite). However, the hysteresis loops of the latter are usually supposed to show "goose-necked" shapes (42, 43), which are absent in our results. This allows us to infer that, even if some of our samples contain hematite, the amount must be limited, which is supported by the following rock magnetic results (Figs. S1*E* and S2) and NRM demagnetization during paleointensity experiments (Fig. 2). The bulk coercivities (B_c values) of the specimens are generally low, with a range of ~10 to ~20 mT, which demonstrates that soft magnetic minerals are the dominant magnetic carriers. The IRM acquisition curves (Fig. S1*E*) either saturate before 200 mT (DXZa and ZJZg) or increase significantly before 200 mT and keep slightly increasing until 800 mT (BJY8b and DQ10v), which supports the inference of soft magnetic carriers to be dominant. The shapes of FORCs (Fig. S1 *F* and *G*) indicate the existence of SD fraction, probably mixed with SP grains (44, 45).

The representative M–T curves show good reversibility (Fig. S2), which indicate that the magnetic carriers are thermally stable. T_c values calculated by the second derivative method described by Tauxe et al. (43) are ~580 °C (ZJZg) or lower (BJY8b, ~540 °C; DXZa, ~570 °C; DQ10v, ~515 °C). The former demonstrates the existence of magnetite, whereas the latter is usually explained as titanomagnetite in most of the previous studies (11, 12, 46, 47). However, we put forward another possibility for those with T_c values less than 580 °C in this study. It was demonstrated that not only titanium (Ti) but also aluminum (Al) substitution can reduce the T_c values of magnetic minerals (48). The SEM images and elemental spectra show the presence of both Ti and Al elements (Fig. S3), indicating both Ti- and Al-substituted magnetic minerals are possible in archaeological materials made of clay minerals. This, combined with the M–T results, suggests that magnetite, Ti-magnetite, and/or Al-magnetite are the dominant magnetic carriers.

249
250
251
252
253
254
255
256
257
258
259
260
261
262
263
264
265
266
267
268
269
270
271
272
273
274
275
276
277
278
279
280
281
282
283
284
285
286
287
288
289
290
291
292
293
294
295
296
297
298
299
300
301
302
303
304
305
306
307
308
309
310

311
312
313
314
315
316
317
318
319
320
321
322
323
324
325
326
327
328
329
330
331
332
333
334
335
336
337
338
339
340
341
342
343
344
345
346
347
348
349
350
351
352
353
354
355
356
357
358
359
360
361
362
363
364
365
366
367
368
369
370
371
372

Fig. S1. (*A*–*D*) Hysteresis loops of representative samples. Red (blue) loop is before (after) paramagnetic correction. B_c, coercivity; B_{cr}, remanent coercivity; M_r, remanent magnetization; M_s, saturation magnetization. Data are analyzed with the software of Pmagpy-2.184. (*E*) IRM acquisition curves of representative samples. (*F* and *G*) FORC plots analyzed with the software of FORCinel_1.17 (49).
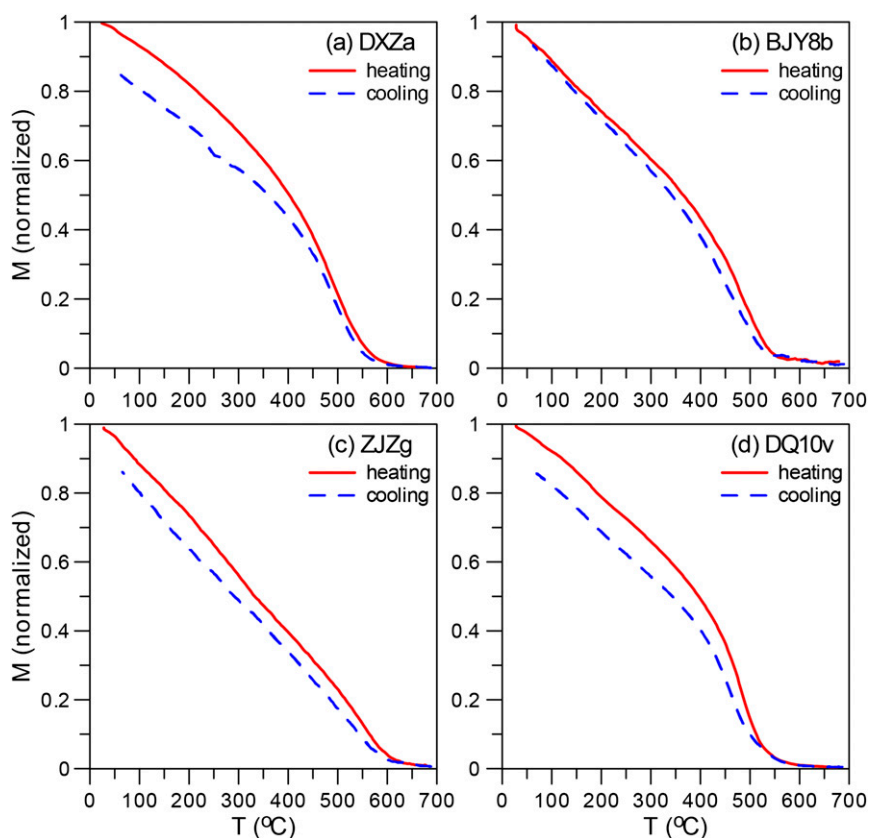
Fig. S2. Representative variations of normalized magnetization versus temperature. Samples are processed in air in an applied field of ~1 T with heating/cooling rates of 30 °C/min. Red solid (blue dashed) line represents heating (cooling) procedure.
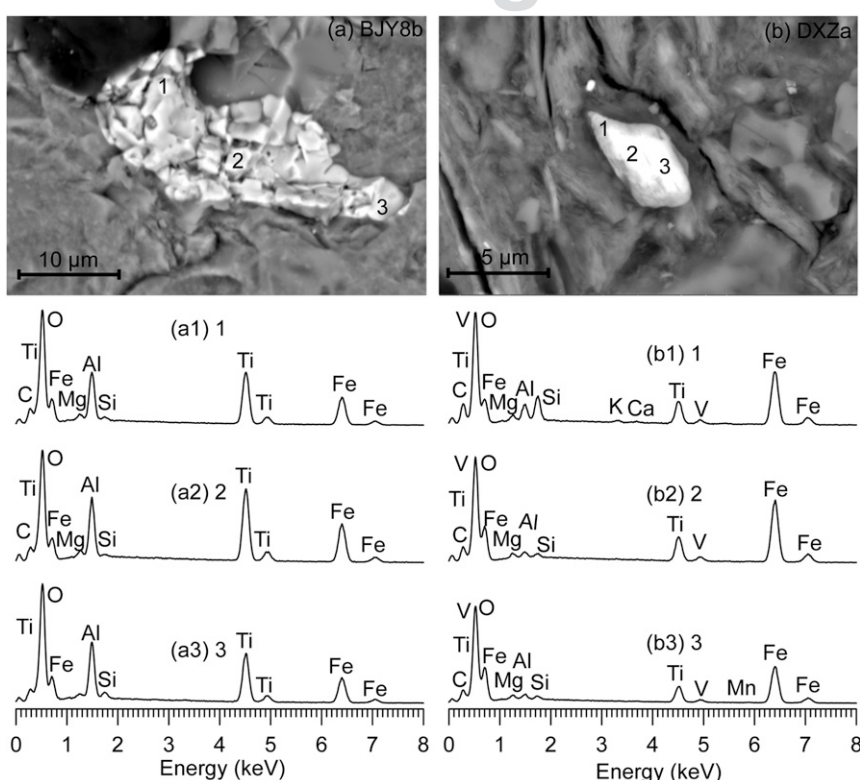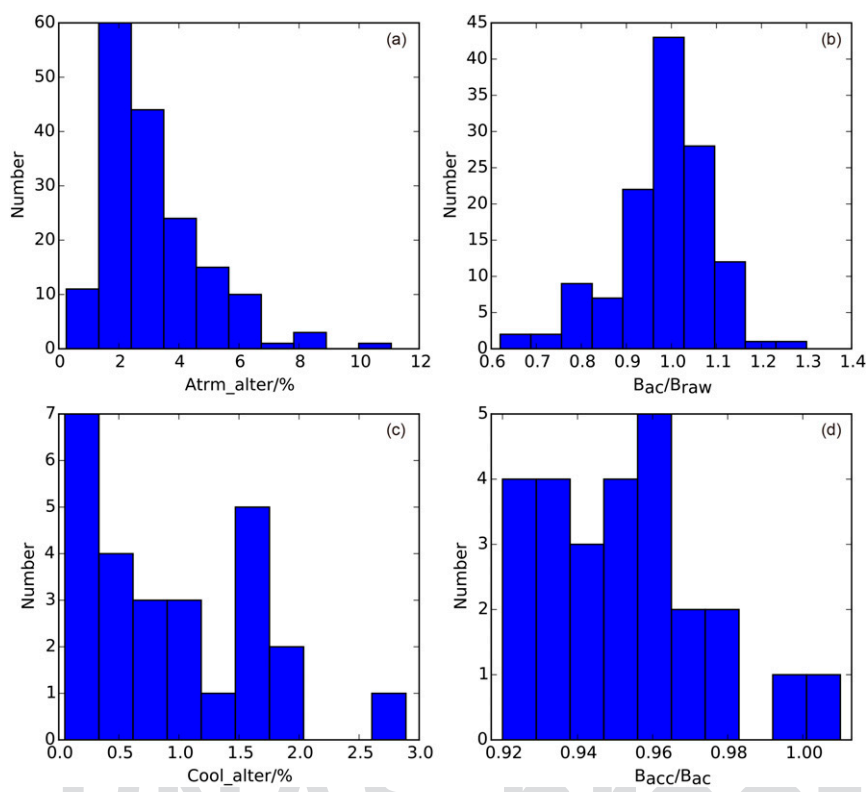

Fig. S3. Scanning electron microscope (SEM) images and energy-dispersive X-ray spectroscopy (EDS) analysis in backscattered electron (BSE) mode.

497
498
499
500
501
502
503
504
505
506
507
508
509
510
511
512
513
514
515
516
517
518
519
520
521
522
523
524
525
526
527
528
529
530
531
532
533
534
535
536
537
538
539
540
541
542
543
544
545
546
547
548
549
550
551
552
553
554
555
556
557
558

Fig. S4. Histograms of (*A*) alteration percentage during the TRM anisotropy correction experiment, which is the maximum difference (expressed as percentage) of the four pairs (+*x*/−*x*, +*y*/−*y*, +*z*/−*z*, and the two +*x* steps) of TRM; (*B*) extent of TRM anisotropy correction described by the ratio of intensity value after anisotropy correction (B_{ac}) to the raw intensity (B_{raw}); (*C*) alteration percentage during cooling rate correction experiment, which is the difference between two fast cooling steps; and (*D*) cooling rate correction factors expressed as the ratio of intensity after both anisotropy and cooling rate correction (B_{acc}) to B_{ac}.

Other Supporting Information Files

Table S1 (DOCX)
Table S2 (DOCX)
Table S3 (DOCX)
Table S4 (DOCX)
Table S5 (PDF)

559
560
561
562
563
564
565
566
567
568
569
570
571
572
573
574
575
576
577
578
579
580
581
582
583
584
585
586
587
588
589
590
591
592
593
594
595
596
597
598
599
600
601
602
603
604
605
606
607
608
609
610
611
612
613
614
615
616
617
618
619
620

AUTHOR QUERIES

AUTHOR PLEASE ANSWER ALL QUERIES

Q: 1_ Per journal style, section headings may not be numbered (except in Mathematics and Applied Mathematics papers). Consequently, the numbers have been removed from the section headings in *Supporting Information*.

Q: 2_ In sentence beginning "To confirm the unusually low paleointensities....": PNAS does not allow claims of priority or primacy, hence the term "new" has been deleted.

Q: 3_ In sentence beginning "The remaining artifacts....": PNAS does not allow claims of priority or primacy, hence the term "new" has been deleted.

Q: 4_ "IGGCAS" has been defined as "Institute of Geology and Geophysics, Chinese Academy of Sciences." Please confirm the definition.

Q: 5_ For Fig. S2 legend: Please cite panels *A–D*.

Q: 6_ For Fig. S3 legend: Please cite panels *A*, *A1–A3*, *B*, and *B1–B3*.